The DELPHI Trigger System at LEP200

V. Canale[1], P. Charpentier[2], J.P. De Wulf[3], F. Fontanelli[4], C. Gaspar[2], R. Goorens[3], C. Lacasta[2], M. Sannino[4] and G. Valenti[2,5]

1 Dipartimento di Fisica Università di Roma "Tor Vergata" and INFN
2 CERN
3 I.I.H.E., B-1050 Brussels,Belgium
4 Dipartimento di Fisica Università di Genova and INFN
5 Sezione INFN di Bologna

Abstract

In this note we describe the hardware and software modifications to the DELPHI trigger complex carried out since the beginning of the high energy runs of LEP. The description of the the trigger configurations and performances for 1998 data taking are also presented.

1 Introduction

Since the increase of the LEP energy in 1995, a number of upgrades and modifications of the Delphi trigger complex [1], have been accomplished. While some hardware interventions were dedicated to replace and rebuild fastbus modules (e.g. the ZEUS mother and daughter boards), major evolution has occurred in the trigger definition mostly dictated by the physics to be addressed at energies above the Z^0. The increase in luminosity and background at LEP2 would have produced untolerable trigger rates had the same redundancy of the trigger used for LEP1 been maintaned. Modifications [2] were therefore channeled towards a reduction in the trigger rate with minimal efficiency loss for standard physics channels and retension of a reasonable sensitivity to potentially new physics.

In this note we review the status of the DELPHI trigger at high energy from the hardware and the efficiency performances viewpoint. In section 2 we describe the modifications that occurred on the architecture (hardware and software), section 3 is dedicated to the trigger "every day life" i.e.: trigger conditions, rates and dead time. In section 4 we discuss the efficiency of the system and section 5 is devoted to some considerations for future runs. Conclusions are drawn in section 6. Several appendices have been included in an effort to provide all the relevant information for a "standard" DELPHI user.

As reminder figure 1 shows schematically the polar angle arrangement of the subdetectors relevant to our trigger system. In Appendix A we briefly recall the list of the subdetector triggers with their mnemonic names used in the text.

2 Architecture update

2.1 Trigger/DAQ control.

At the acquisition timing and control level, the ZEUS mother, daughter and fan-out boards have been replaced and a complete set of spare modules are now available. The new PANDORA modules are also operational since 1997 on all detectors. A new system to synchronize with the LEP machine bunches, based on the injection synchronization signal, is under study.

2.1.1 The ZEUS Board

The Delphi Trigger Supervisor Control Box [3], ZEUS has the task of controlling the timing of the experiment. A new version of this module, called NEW ZEUS, has been built in order to exploit all the new characteristics of the "NEW PANDORA" [4] modules. The NEW ZEUS has fundamentally the same functionality as the former module, i.e. the signals exchanged with the external world are essentially the same and follow the same protocol. An important added feature is the capability to synchronize with 4,8,16 bunches in the "internal" timing. The timing signals relevant for the external world are not any more generated as combinatorial functions of the input signals, as in the former module, but are produced as output functions of a synchronous "state machine" operated with a 20 MHz clock. The sequences of the state machine is controlled by the trigger decisions generated by the PYTHIA look-up tables.

2.1.2 The ZEUS Daughter Board

A new Zeus daughter card [7], based on modern electronic technology, has been designed to complement the new capabilities of the ZEUS card. A prototype has been successfully tested in 1997. A feature of the new card is the option to run in several bunch modes (4,8,16) in both internal and LEP RF. Moreover the card gives the possibility to monitor, without disturbing the data acquisition, the most important timing signals i.e. the pick-up, the BCO and the radio frequency.

2.1.3 New PANDORAs

Since the 1996 run, new Local Trigger Supervisor Decision Box modules (vulgarely called PAND2) have replaced (one per "detector" for a total of 28) the original (sin!) "Pandoras". These modules supervise the timing of all partitions in the Delphi detector. Each module consists of a mother board, three PLL, three "burst", one RF, one Fastbus coupler/state machine and one warning/delay daugther boards:

- PLL: (phase locked loop) synthesizes the clock frequencies,
- Burst: produces the burst/free_running clocks,
- RF: produces the internal RF3,
- Fastbus coupler/state machine for Fastbus communication protocol and control of the trigger cycle,
- Warning/delay: generates the programmed warnings and clock delays.

Characteristics and operation details can be found in [8], [9]. Results from extensive tests conducted prior to installation are described in [10].

2.1.4 Central Timing and Pick-up System

During the 1997 run some desynchronizations have been observed in the TPC detector. The pick-up signals from positrons and electrons [1] are capacitive signals taken from probes placed near the beam at the level of the quadrupole near the DELPHI interaction region. After transmission to the B2 barrack the signal is discriminated and its delay with respect to RF is adjusted. The strong dependence of the signal strenght and shape on the the beam position and intensity is a plausible cause of the observed instabilities. A first stabilization of the pick-up signal amplitute has been achieved by summing analogically the capacitative signals from two probes located at 180 degrees with respect to the beam. This significantly reduced the instabilities related to the correlation between signal strength and beam displacements.

As second step and major improvement we would use the synchronization injection signal of the LEP itself. This signal is extremely stable and distributed on each radio frequency stage. A new connection form the closest RF station and the corresponding control electronics have been installed and we plan to test it against the present system.

[1] For the central timing the relevant pick-up is the e^- signal while the e^+ is monitored.

2.2 Trigger Decision.

The main modification was the replacement of the DECODER BOX module and the rearrangement of the scaler monitoring system.

2.2.1 The DECODER BOX Module

The DECODER BOX receives the trigger data lines (TDL) from all detectors that can provide a trigger and dispatches one sets of signals to the trigger processors (PYTHIA I and II levels) and another set to the the scaler system where the TDLs rates are monitored. The new DECODER BOX [6] has been installed in 1996. For each level the 120 TDL's are send to a total of 8 input cards (16 channels each)[2], these lines are then split:

- a copy of the TDLs is sent to trigger look-up-table (PYTHIA) receivers, after possible channel masking;
- another copy is send to the scaler system. On these lines it is possible to apply a decoding operation on each pair of channels. Due to the original design, the TDLs of each detector generally give the multiplicity coded on two lines. The decoding operation to construct the majorities 1 and 2 can be software activated on each line pair before sending it to the scalers.

The system can be accessed in read-write mode via FASTBUS to set the masking and decoding options, as described in section 2.3.1.

The control of the power supply for the DECODER BOX modules has been inserted in the general SLOW CONTROL in order to monitor the status of the crates.

2.2.2 The SCALER System

One FASTBUS crate is reserved for a set of 13 scaler modules for online monitoring. Each scaler contains 32 (2*16) independent channels that provide 32 bits of scaling. The arrangement of the channels has been changed with respect to [1] in order to match the requests of the new decoder box outputs and the disappearance of the old NIM trigger signals. The current mapping is the following:

- 8*16 channels are devoted to PYTHIA first level inputs;
- 8*16 channels are devoted to PYTHIA second level inputs;
- 10*16 channels are devoted to monitor backgrounds, luminosity etc...

One of the major advantage of the new decoder box is the possibility to monitor all the PYTHIA inputs both at first and second level. The detailed description of the scaler map can be found in the file on the online cluster
delphi$online:[trigger.monitoring.scal_status.source]scaler_db.dat

[2] 8 input channels of the DECODER BOX are not send to PYTHIA but only to the scaler system and can be used to test the rates of new TDLs.

2.3 The Central Software

Some modification have occurred in the central software of the trigger system. A new version of the former "OLYMPUS" program, called PCP (Pythia Control Program) [11] includes the new masking-decoding features of the DECODER BOX.

2.3.1 Pytha Control Program (PCP)

PCP is a stand alone program that can perform several controll and monitoring tasks for the trigger system.

While the control operation corresponding to Zeus and the trigger Pandora are restricted to experts, the monitoring and setting of the mask registers of both Pythia 1st level and 2nd level, as well as the decoding masks for our scaler system, can be operated by the Delphi DAS shifter.

The graphic interface SMG is used to execute the program on any terminal/workstation. The program is started by typing PCP (symbol pointing to the proper version) and following the menu structure. The TDL (Trigger data lines) maps should however be consulted when changing mask registers and/or scaler decoding. These maps are available from the trigger account on any machine of our online cluster by typing: **$set def trigger:[fastbus.pythia.programmer.luts]** (to go to the correct directory) then look at the text files **PYTxx_T1.DAT and PYTxx_T2.dat** where xx stands for the year two digits (i.e. ..97,98..).

2.3.2 Setting of the Trigger Conditions

The operation of PYTHIA has not been changed, the setting of the trigger conditions is done by loading the PYTHIA tables as described in [12].

Some features have been introduced to better handle the calibration and test triggers:

- to apply a fixed down-scaling factor (from 1 to 255) to a specific Decision Function;
- to apply automatically a variable down-scaling factor to a specific Decision Function in order to keep its rate constant;
- to switch ON any specific Decision Function as soon as the global rate is below a defined value.

The handling of these features is described in the Appendix B.

2.3.3 The Trigger display

A Trigger display is available and included in the DUI package [13]. This display allows the visualisation of the main trigger quantities like the rate of each Pythia function for both levels and whenever possible (availability in the scalers) the rate of each component of every function. It also allows control functions like loading Pythia tables, setting prescaling factors, enabling/disabling functions, etc.

Other displayed quantities are the experiment's livetime, sub-detectors readout times and the overall trigger system status.

The limits between which a trigger function can oscillate are defined in a configuration file so that the function's value is displayed in green for normal behaviour and orange or

red when outside the limits. The Trigger display is started by the command:
$dui trigger.

2.3.4 The SCALER monitoring

The SCALC program has been adapted to the new scaler map and it is maintened to run on alphanumeric terminals (i.e. the Falco terminals down in the pit) where the magnetic field does not allow the use of graphics. Before running SCALC on a VMS machine a few preliminary operations should be done, these are :
$@delphi$online:[trigger]setup
$define tp$scalc_src delphi$online:[trigger.monitoring.scal_status.source]
and then
$scalc

An alternative monitoring program based on DUI (DELPHI User Interface)[13], is also available and can be used on graphic terminals. It is started by
$dui scalers
The detailed description of the program and the way to operate it can be found in [14].

3 Trigger Conditions

The trigger conditions are set with two goals in mind: 1) maximize the efficiency for standard physics channels, 2) keep enough sensitivity to potentially new physics. The acquisition of an event is decided on the basis of the two successive synchronous levels. A third level trigger [15], asynchronus with the acquisition, validates events before writing on permanent medium. The latter uses the same logic of the second level complemented with more detailed quantities derived after data read out. Since 1997 a fourth level trigger [16] has also been introduced with the mandate to eliminate "empty" events. Only first and second levels are relevant for the online life (rates, dead-time etc...). The third and fourth levels reduce the number of events to be processed offline.

3.1 Configuration During the High Energy Runs

Two sets of trigger conditions were used during the high energy runs, one for physics events and one for calibration.

3.1.1 First Level Physics Triggers

At first level, the trigger condition for physics events is any of the following:

- at least one track in ID, OD, TPC or FCH;
- at least one electromagnetic shower in HPC or FEMC;
- at least one hadronic shower in HCAL;
- at least one track in the barrel muon chambers;
- a coincidence between forward and backward scintillators (HOF);
- a back to back coincidence for barrel scintillators (TOF);

3.1.2 Second level physics triggers

In general detectors have separate first and second level processors [3]. At second level the trigger conditions generally involve coincidences between different subdetectors. Any of the following configuration will trigger:

- **at least a track in the barrel, forward or backward regions**. To moderate the rate in forward (backward) angular regions only coincidence of detectors are considered. The detailed components are shown in table 1.
- **at least a shower in the barrel region**. This trigger from HPC uses the second level data in azimuthal correlation with first level results. The concidence between TOF and HPC first level was also used in the trigger as back-up solution;
- **at least a shower in the forward or backward regions**. This is obtained using the high threshold ($\sim 5GeV$) of the FEMC detector;
- **at least a neutral shower in the STIC**. This trigger has been very usefull in the high energy runs to identify the radiative return followed by invisible decays of the Z. Neutral showers in the STIC are validated by veto counters covering the geometrical acceptance of the calorimeter. The same trigger is active at first and second level. Detailed description and performances can be found in [31];
- **at least two showers in the barrel region**. This trigger is conceived for multi-photons final states, it is obtained from the HPC first level processor transported to second level. The energy threshold and geometrical acceptance are somewhat different from the single photon barrel trigger;
- **at least a shower in the HCAL anode readout**. The hadron calorimeter anode read-out [28], implemented during 1997, is used as complementary trigger for exhotic searches. This trigger has a dedicated first level pre-trigger.

Trigger for low P_T tracks . This trigger was conceived to enhance the sensitivity to potentially new physics channels [4] where small visible energy is deposited in the detector. These topologies are also very frequent in $\gamma - \gamma$ events. For the barrel region the trigger consisted of a global coincidence between ID and OD. The resulting transverse momentum cut is $\sim 700MeV/c$. For the forward-backward regions a multiplicity greater-equal than 2 was required in the TPC-RZ trigger processor. These componets were crucial during the 1995 run at $\sqrt{s} \sim 135GeV$ in the detection of the f' resonance. Unfortunately the increase of the background at higher energy forced us to abandon this trigger during 1998 data taking.

[3] In several cases this is not true and the first level signals are used at second level (e.g. the hadron calorimeter, the forward-backward chambers).

[4] Several SUSY scenarios may involve such topologies.

Barrel Region	Forward Region	Backward Region
TPC CTG	ID*HAFW	ID*HABW
ID*OD (TPC cracks)	ID*MUFW	ID*MUBW
ID*OD*HABL	TPCFW*EMFW	TPCBW*EMBW
ID*OD*MUBL	TPCFW*MUFW	TPCBW*MUBW
	TPCFW*HAFW	TPCBW*HABW
	TRFW*EMFW	TRBW*EMBW
	TRFW*MUFW	TRBW*MUBW
	TRFW*HAFW	TRBW*HABW

Table 1: Components of the single track trigger at second level

3.1.3 Calibration and Test triggers

Several calibration and test triggers are foreseen for the monitoring of the detectors. These components are usually active at first level and then transported to second level to trigger the acquisition. They are:

- **the STIC BHABHA trigger**. It is the fundamental tool for the luminosity measurement. At higher energy the precision required is less important than at LEP1 therefore this trigger is usually downscaled by a factor 3;
- **the VSAT BHABHA trigger**. This is the luminosity trigger with the BHABHA events at very small angles;
- **the STIC single arm trigger**. This component is relevant to evaluate the efficiency of the BHABHA trigger and to cross check the small angle neutral trigger. At the level of the central system this trigger is automatically downscaled in order to keep its rate under $\sim 0.3Hz$;
- **the parallel muon trigger**. It is obtained by the coincidence of the forward and backward muon chamber quadrants in parallel (with respect to e+ e- beams) topology.
- **the TPC laser trigger**. This is a dedicated trigger for TPC laser calibration [32], the rate is adjusted to $\sim 0.01Hz$;
- **the random trigger**: usefull for test and to run the acquisition when there is no beam in LEP. It is obtained with a radioactive source (Fe 55).

3.2 Trigger Rates, Dead Time and Time Stability

An important effort has been devoted to reduce the experiment dead time. The fraction of dead time introduced by the trigger can be expressed as function of first and second level trigger rates by the formula:

$$\alpha_{Trigger} = \nu_{LEP}^{-1} (N_{lost}^{T1} * (T1 - T_{VSAT}) \quad + 2 * N_{lost}^{T1} \;\; T_{VSAT} \quad + N_{lost}^{T2} \;\; T2)$$

where ν_{LEP} is LEP rate crossing and $T1, T_{VSAT}, T2$ are first, VSAT [5] second level trigger rates. $N_{lost}^{T1,T2}$ are the number of LEP crossing lost due to a T1 yes and a T2 yes. They are given by:

$$N_{lost}^{T1} = 1 \; (4 \; bunch \; mode), \;\; 3 \; (8 \; bunch \; mode) \;\; per \; T1 \; yes$$

$$N_{lost}^{T2} = (\Delta_{read-out} \; \nu_{LEP}) \sim 100 \; (4 \; bunch \; mode), \;\; 200 \; (8 \; bunch \; mode)$$

where an average $\Delta_{read-out} \sim 2.5ms$ has been used. For the standard running of LEP in 4 bunch mode at high energy we obtain:

$$\alpha_{Trigger}(\%) \approx 0.0022 * T1 \quad + 0.22 * T2$$

where we have neglected the contribution of the VSAT ($T_{VSAT} \sim 1Hz$).

The trigger rate is naturally a function of background which in turn depends on the current in the machine. In figure 2 we report the trigger rates at first and second level as function of the total current in LEP. The plots correspond to typical fills of the different periods of high energy runs from 1996 to 1998 ($\sqrt{s} = 160, 174, 183$ *and* $189 \; GeV$). The trigger rates and dead times, as function of the fill time, are shown in figure 3 for a typical 1998 high energy fill. The variation of the trigger induced and total dead time versus the current is shown in figure 4. In standard conditions the dead time introduced by the trigger rate is rather small $\alpha_{Trigger} \approx 2 - 3\%$.

The data to monitor the online performance of the trigger system (rates) are stored in an n-tuple on a fill by fill basis. The n-tuple has one entry each 10 seconds. These files are stored in the online cluster area **delphi$data:[tp.ntuples]**.

The time stability of our system is systematically monitored with trace plots versus (solar) time of trigger rates, dead time, read-out time, etc.

The evaluation of the efficiency of a specific trigger component is obtained by selecting a sample of events triggered by, beside the one under study, one or more independent trigger components. Systematic offline analysis of trigger efficiency [6] is performed continuously on limited amounts of integrated luminosity (the typical "quantum" is $\sim 1pb^{-1}$ in order to have sufficient statitistics). Examples of this efficiency/stabilities are shown in figures 5, 6 and 7. Since 1998 this procedure has been automatized in the central offline data quality checking [33]. Plots are updated day by day and may be found at the following web address:
http://delphiwww.cern.ch/~chkprod/delwww/98HC/trace/

[5] The VSAT trigger has a dedicated processor with a dead time $\sim 80\mu s$. The standard T2 processor dead time is $\sim 39\mu s$.

[6] See the Section 4 for definitions and computation.

4 Trigger performances

4.1 Trigger efficiencies

4.1.1 Efficiency estimation

A description of trigger efficiency determination can be found in [34]. To estimate the efficiency a sample of events sensitive to one or more independent triggers, beside the one we want to compute the efficiency, is selected. Calling N_{TOT} the total number of events and N_{obs} the subsample triggered by the component under study, the efficiency ϵ is extimated according to:

$$\hat{\epsilon} \ = \frac{N_{obs}}{N_{TOT}}$$

In case of redundancy when two trigger components (A and B) are present, calling:

$$\begin{aligned} N_A &= \textit{number of events triggered by A} \\ N_B &= \textit{number of events triggered by B} \\ N_{AB} &= \textit{number of events triggered by both A and B} \end{aligned}$$

the efficiencies of the two components and the global efficiency are given by:

$$\hat{\epsilon_A} \ = \frac{N_{AB}}{N_B}, \ \hat{\epsilon_B} \ = \frac{N_{AB}}{N_A}$$

$$\hat{\epsilon} \ = \epsilon_A + \epsilon_B - \epsilon_A \ \epsilon_B \ = \frac{(N_A + N_B - N_{AB})}{\frac{N_A N_B}{N_{AB}}}$$

The generalization to the case of more independent components is described in [1].

In the DELPHI trigger configuration for LEP1, the logic combinations of subdetectors induce correlations between the trigger components. The way to handle properly this situation was described in [1]. At LEP2 a substantial reduction of the trigger components was necessary to moderate the acquisition rate. The trigger conditions described in section 3.1 show a clear separation between independent parts of the detector, in particular the forward, barrel and backward regions are now distinct and can be used as independent components in the evaluation of the efficiency. This separation is present at both first and second level and this automatically takes into account correlations betwen the different trigger levels.

Even if reduced with respect to LEP1 configuration, redundancy is still present and it is exploited to compute efficiency for event topologies involving only one geometrical region of the detector and prevent inefficiencies from eventual subdetector malfunction.

The definition of the efficiency $\hat{\epsilon} \ = \frac{N_{obs}}{N_{TOT}}$ naturally implies the use of the binomial distribution for the uncertainty estimation. For large samples of events the normal approximation holds and the variance can be used to estimate the errors:

$$\hat{\sigma} \ = \sqrt{N_{TOT} \ \hat{\epsilon} \ (1 - \hat{\epsilon})}$$

$$\Delta\hat{\epsilon} = \frac{\hat{\sigma}}{N_{TOT}}$$

Nevetheless this approach is unsatisfactory for small size samples and/or for "very efficient" components for which if $\epsilon \to 1$, then $\Delta\epsilon \to 0$. This situation is present in the actual data due to the limited statistics at LEP2 and to the good performances of the trigger system. In such situation the efficiency uncertainty should be estimated with the general confidence interval approach which automatically takes into account the carachteristics of the binomial distribution and the sample size.

The foundation of the method is described in [35]. The measurement x_m, deriving from probability distribution function (p.d.f.) $f(x, \epsilon)$, is used to estimate the unknown parameter ϵ. To construct the confidence interval $[\epsilon_{min}, \epsilon_{max}]$ with probability content[7] α we must solve the following equations with respect to $\epsilon_{min}, \epsilon_{max}$:

$$F(x_m; \epsilon_{max}) = \frac{1+\alpha}{2}, 1 - F(x_m; \epsilon_{min}) = \frac{1+\alpha}{2}$$

where $F(x, \epsilon)$ is the cumulative distribution. The solution of the system is illustrated graphically in figure 8. In the case of the binomial distribution, due to the discontinuty of the p.d.f. and the mathematical accuracy in the solution, the equality sign is replaced by less or equal. In figure 9 we report the 68% confidence belt for the binomial distribution with total number of events $N = 5, 10, 50$ *and* 100. The error, computed using the variance of the binomial distribution, is superimposed on the same figure. The normal approximation is satisfactory for large samples (a part for the limits $\epsilon \to 0, 1$), and will be used in the analysis for sample size $N \geq 100$.

4.1.2 Subdetector and global efficiencies

In the DELPHI system several signals from different subdetectors are combined to form the trigger conditions. From the physics analysis point of view, it is natural to define subdetector efficiency corresponding to the response to a specific topology (e.g. the muon chamber trigger response for tracks identified as muons in the offline analysis), in particular single tracks [8] inside the geometrical acceptance of the subdetector and with special identification requirements from the offline analysis:

- muon identification for the muon chambers;
- electron identification for the electromagnetic calorimeter;
- electron and muon veto with pion signature in the Rich for hadron calorimeters;
- no special requiremenmt for tracking devices.

These efficiencies are reported in figures 5, 6 and 7.

The subdetector efficiencies cannot be directly translated into efficiencies of the trigger system. To estimate the actual efficiency one has to consider as trigger components the different logical combination of trigger signals described in section 3. The results for several event classes of physical interest are described in the following.

---
[7] Usually the central interval at 68% level is choosen.

[8] See section 4.4 for the definition of this topology and the criteria used to trigger it independentely

4.2 Single track efficiency

It is important to estimate the trigger efficiency on isolated tracks as function of their momenta and geometrical direction. This results can be used to obtain the trigger efficiencies for physics channels involving low track multiplicities and low momentum tracks. This is the case for several $\gamma - \gamma$ events and eventually for some SUSY scenarios (e.g. the degenerate heavy chargino production with small release of visible energy in the apparatus). To estimate these efficiencies the sample is obtained selecting isolated tracks in the following angular regions:

- forward $10^o \leq \theta \leq 35^o$;
- barrel $45^o \leq \theta \leq 135^o$;
- backward $145^o \leq \theta \leq 170^o$;

The independent selection is ensured by requiring a track (trigger) activity in the complementary regions. Figure 10 shows the efficiencies as function of the transverse momentum of the single track in the different angular regions. The angular θ and φ efficiencies are shown in figure 11 (for these tracks a kinematical selection has been applied: (a)$P_T \geq 1$ GeV in the barrel, (b)$P_T \geq 3$ GeV in the forward/ backward region.).

We also define two intermediate regions:

- forward-barrel $30^o \leq \theta \leq 50^o$;
- backward-barrel $130^o \leq \theta \leq 150^o$;

where specific detector superposition is used in the trigger. Results for these intermediate regions are shown in figure 12.

4.3 Single shower efficiency

Trigger efficiency for single shower can be derived in analogy with the single track topologies. We select events having an isolated track identified as an electron in the following angular regions:

- forward $10^o \leq \theta \leq 35^o$;
- barrel $45^o \leq \theta \leq 135^o$;
- backward $145^o \leq \theta \leq 170^o$;

As usual an independent triggering of the event is also required. Efficiencies for these regions are shown in figure 13 as function of the electron energy.

4.4 Efficiency for Leptonic and Hadronic Events

4.4.1 Leptonic events

The dilepton sample consist of (e^+e^-) and $(\mu^+\mu^-)$ identified requiring standard DELPHI cuts [36] and collected during 1998. The event polar angle is defined as the average $\theta = (\theta^+ + \pi - \theta^-)/2$ this turns out to be a good approximation since the acoplanarity is peaked around $\Delta\theta \sim 0^o$. Defining θ between the pairs as the smallest between $[0^o, 90^o]$, two acceptance regions are considered:

- Low θ region $15^o \leq \theta \leq 35^o$
- High θ region $40^o \leq \theta \leq 90^o$

For the high θ region two independent triggers in the barrel can be used, while for the low θ region we use as independent components the forward and backward triggers. Table 2 summarizes the choice of the independent triggers for the two classes of leptonic events and two angular regions. The efficiency for leptonic events as function of θ is reported in figure 14(a,b).

4.4.2 Hadronic events

For the hadronic events the selection is described in [36]. For this topology the event polar angle is taken to be the thrust axis. Similary to the leptonic events two θ-regions with independent trigger components are defined in order to determine the efficiency for hadronic events as function of the thrust angle θ_{THR}. Typical results are reported in figure 14(c).

Event Topology	Component A	Component B
$e^+ - e^-$	TPC CTG	HPC II level
$\mu^+\mu^-$	TPC CTG	ID*OD*(MUBL+HABL)
$Hadronic$	TPC CTG	ID*OD*(MUBL+HABL)

Table 2: Independent components in the barrel region for leptonic and hadronic events

4.5 Efficiency for two high momentum track events

At the energy of LEP2 the two significant processes of W^+W^- pairs production and the radiative return to the Z resonance are characterized, in the leptonic channels, by topologies with two high momentum tracks with significant acoplanarity. Then the efficiency computation of the previous section has to be modified by selecting events with two tracks of momentum greater than 10 GeV in the following topologies:

- both tracks in the barrel region (BRL-BRL);
- both tracks in the forward (backward) region (FWD-FWD);
- one track in the barrel and the other in the forward (backward) region (BRL-FWD);
- one track in the forward and the other in the backward region (FWD-BWD);

and requiring in the regions complementary to those containing the high momentum tracks, the presence of a track and the corresponding "firing" of the trigger component. This ensures the independent selection of the event. The efficiency is therefore derived separately for the four classes (BRL-BRL), (FWD-FWD), (BRL-FWD) and (FWD-BWD). The trigger efficiencies for these event topologies as function of the momentum cut for the data collected during the 1998 run, are reported in figure 15.

5 Perspectives for the Future Runs

In the next two years of running, the LEP energy will increase up to $\sqrt{s} \sim 200GeV$, with a maximum current of up to 8 mA. We expect, therefore, an increase of the background reflected in turn in an increase of the trigger rate and hence higher dead time. To avoid, as much as possible, trigger induced dead time, alternative/modified trigger conditions have been studied during the last period of 1998 data taking.

At first level:

- the logic of TPC-RZ trigger has been modified to reinforce the single track counting algorithm by requiring correlation with the "shadow" trigger [18];
- the ID.OR.OD component which correspond to $\sim 40\%$ of the total T1 rate, has been changed into the coincidence ID.AND.OD. OD dead regions will be cured by requiring the presence of ID only in the corresponding angular ranges.

The effects of these modifications on the trigger rate are shown in figure 16 for the various components and for the total first level. In figure 16(d) the induced dead time is reported as function of the circulating electron/positron beam currents. Also shown is a "tentative" extrapolation to a total current of $\sim 8mA$ which might be a realistic scenario for future years[9].

We have studied the effects of this new configuration on the single track efficiency. Comparison of efficiencies between "old" and "new" configuration are shown in figure 17 and 18 for the different angular regions. They suggest that:

- in the forward and backward regions there are almost no losses;
- in the barrel region losses are marginal, and the OD dead zone $\varphi \sim 100^o$ is well recovered;
- in the intermediate regions, affected by the reduced angular acceptance of the OD, the losses seem tolerable.

For the time being no hardware intervention have been envisaged to reduce the second level rate. Possible interventions, which will not alter the philosophy of the trigger, are:

- the increase of the thresholds in electromagnetic calorimeters;
- the increase of the P_T cut in the TPC contiguity;
- further prescaling of the calibration triggers see 3.1.3;

6 Conclusions

We have presented the modifications which occurred in the DELPHI trigger complex since the beginning of the high energy runs of LEP. The configuration of the trigger conditions has been discussed and the performances for the 1998 data taking have been shown. Very good efficiency and acceptable rates have been obtained. Some possible modifications in the trigger logic for improvements in the future runs have also been considered.

[9]This result assumes naively the same backround conditions at higher energy.

Acknowledgements

We would like to thank all our DELPHI colleagues involved in the data taking and in the detector activities for their continuous help during the running periods.

References

[1] V.Bocci et al., NIM A362(1995)361

[2] see the DELPHI Review Workshops from 1995 to 1997

[3] L.Cerrito et al., DELPHI 86-106

[4] V.Bocci et al., DELPHI 96-10 DAS 171

[5] L.Cerrito, DELPHI 90-12

[6] J.P. Dewulf et al., DELPHI 96-177 DAS 183

[7] J.P. Dewulf, DELPHI Note in preparation

[8] V. Bocci et al., DELPHI 96-10, DAS 171

[9] Ph. Charpentier et al., DELPHI 96-9, DAS 170

[10] V. Bocci et al., DELPHI 96-16, DAS 172

[11] G.Valenti, private communication

[12] V.Canale and G. Valenti, DELPHI 92-15 DAS 122

[13] M. Donszelmann et al., DELPHI 92-150 DAS 134

[14] V.Canale et al., DELPHI 96-74 DAS 178

[15] Ph. Charpentier, DELPHI 94-123 DAS 159

[16] B. Bouquet et al., DELPHI 93-29 DAS 141

[17] A.J. Naddox et al., LUCIFER: The DELPHI OD LTSDB (unpublished)

[18] P. Courty et al., DELPHI 89-29 DAS 98

[19] G. Darbo et al., NIM A257(1987)567

[20] T. Kkrevzberg et al., DELPHI 88-51 DAS 84

[21] M. Breussers et al., DELPHI 86-49 DAS 34

[22] J. Buytaert et al., DELPHI 91-61 TRACK 65

[23] F. Spiriti et al., DELPHI 90-27 CAL 74

[24] V. Bocci et al., DELPHI 90-14 DAS 104

[25] L. Lanceri et al., DELPHI 88-8 CAL 55

[26] A. Benvenuti et al., DELPHI 94-31 CAL 112

[27] P. Eerola, DELPHI 89-48 CAL 67

[28] Hadron Calorimeter Group, private communication

[29] J.M. Benlloch et al., NIM A290(1990)327

[30] J. Buytaert et al., DELPHI 88-92 DAS 90

[31] P. Ferrari and V. Hedberg, DELPHI 98-49 CAL 141

[32] TPC Group, private communication

[33] W.J. Murray, DELPHI 98-32, GEN 175, PROG 230
F. Cossutti et al., DELPHI Note in preparation

[34] A.G. Frodesen et al., Probability and Statistics in Particle Physics. Universitetforlaget.

[35] W.T. Eadie et al., Statistical Method in Experimental Physics, North-Holland

[36] DELPHI Collaboration: P. Abreu et al., NIM A378(1996)57

A Appendix: Trigger Subdetectors

We briefly recall the subdetectors contributing to the trigger system of DELPHI. Their angular acceptance is reported in figure 1. The mnemonic names used throught the paper will be recalled.

A.1 Tracking system

The tracking subdetectors contributing to the trigger system are:

- the Inner and Outer detector. These detectors provide both individual triggers (ID,OD) and their φ-correlated coincidence (TRBL) [17];
- the Time Projection Chamber produces triggers at both first and second level. At first level the information from wires is used to form the barrel TPC-RZ [18], the forward (TPCFW) and backward (TPCBW) track triggers. At second level the main contribution is from the contiguity processor TPC-CTG [19] which uses the pad information to reconstruct tracks. This trigger has an intrinsic transverse momentum cut which can be set by software. For part of 1997 and 1998 run it was set to $\sim 0.8 Gev/c$, since september 1998 it has been raised to $\sim 1.2 Gev/c$;
- the Forward Chambers A and B are combined to produce a track trigger [20] in the forward (TRFW) and backward (TRBW) regions. This trigger is available at first and second level;
- the muon chambers produde triggers for penetrating tracks in the barrel (MUBL), forward (MUFW) and backward (MUBW) regions. The trigger is available at both level for the barrel region (MUBL) [21], at second level only for the forward-backward (MUFW, MUBW) sector [22].

A.2 Calorimeters

The calorimetric detectors contributing to the trigger system are:

- the barrel electromagnetic calorimeter HPC. At first level [23] the trigger is obtained from the dedicated scintillators inside the calorimeter (HPC). At second level (EMBLCOR) the collected charge is used to reconstruct showers and the trigger is obtained from a correlation [24] between the scintillators and the observed charge;
- the forward-backward electromagnetic calorimeter FEMC produces triggers in the low angular region (EMFW, EMBW) [25]. The signal is available at first level with two different thresholds;
- the STIC calorimeter [26] is used for the Bhabha events selection and for the single photons at very low angles [31];
- the HCAL cathode readout electronics produces the trigger for the three angular regions: fowrard (HAFW), barrel (HABL) and backward (HABW). Furthermore in 1997 the anode read-out electronics of the calorimeter has been commissioned and constitutes a high threshold dedicated trigger (HACSPEC) [28].

A.3 Scintillators

Finally some fast trigger information is obtained from scintillation counters:

- in the barrel region, TOF [29];
- in the forward regions, HOF [30];

B Appendix: Trigger Condition Settings

The trigger condition setting is established automatically via software. The system takes from a dedicated file in the online cluster the LUTs to be charged, the prescaling factors, etc... An example of such file is:

```
DETECTOR$SPECIFIC:[FASTBUS.PYTHIA.PROGRAMMER.LUTS.LOG]PYTHIA_LOADING.DAT

TRG87_T1
TRG85_T2
1111111111111111            LEVEL  I ENABLE MASK
1111111111111111            LEVEL II ENABLE MASK
 200   1   2   4   1   1   1   1   1   1   1   1   1   1   1   1
   4   3   1 255   1   1   1   1   1   1   1   1   1   1  50   1
CCR    3   0.3              STIC single arm
CCR   14   0.15             MUPARAL
CCR   15   0.3              COSMOLEP TRIGGER
```

The first two lines indicate the LUT number that are loaded at first and second level. The following lines give the mask enable pattern for the trigger processor decision functions (DF), and the prescaling factors to be applied (one line per level). The subsequent lines establish, for dedicated functions at second level, the maximum tolerable rate (in Hz). If the rate is exceeded the system will increase automatically the prescaling factor to limit it.

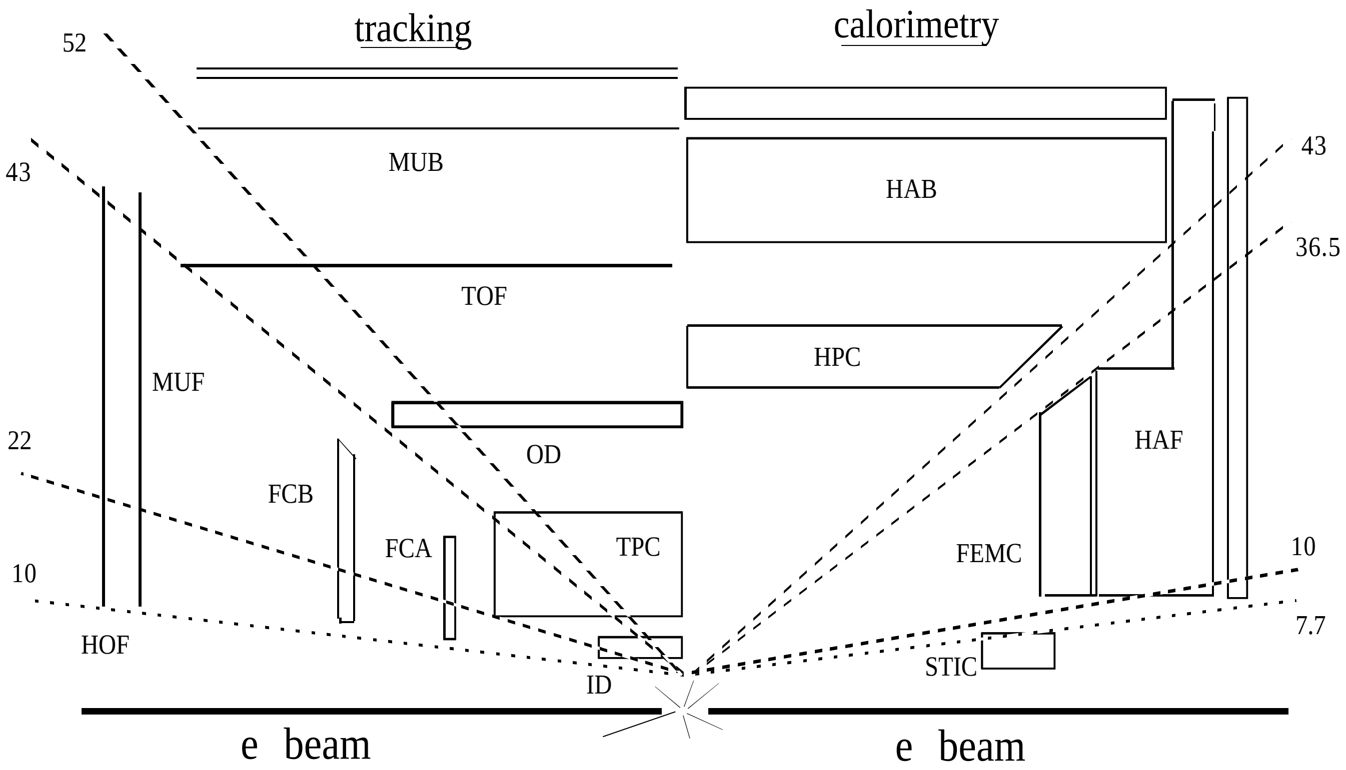

Figure 1: Subdetectors participating in the first and second level trigger and their polar angle acceptance in degrees.

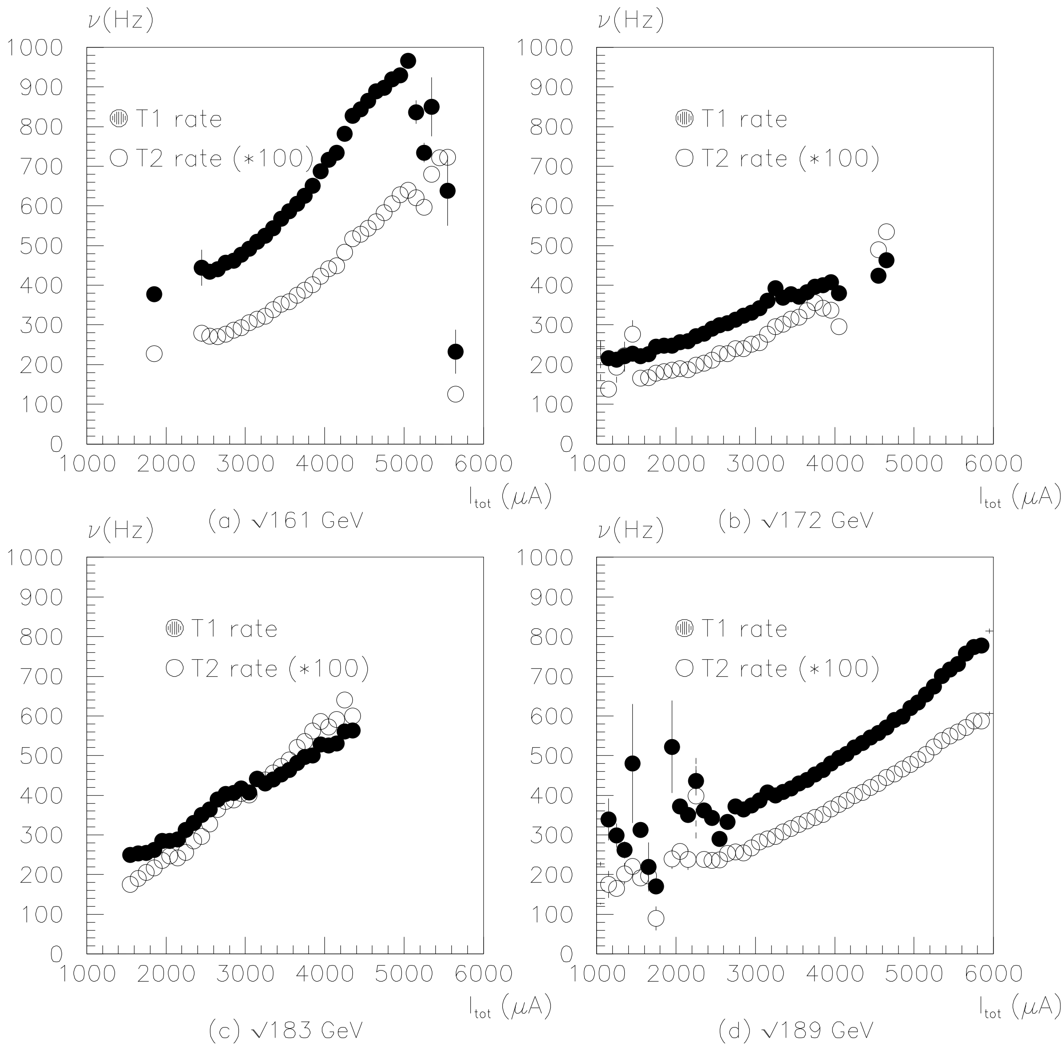

Figure 2: Rates of first (T1) and second (T2) level triggers as function of the total current in the machine for the high energy runs of LEP: (a) $\sqrt{s} = 161\ GeV$, (b) $\sqrt{s} = 171\ GeV$, (c) $\sqrt{s} = 183\ GeV$, (d) $\sqrt{s} = 189\ GeV$. The T2 rate has been multiplied by a factor 100.

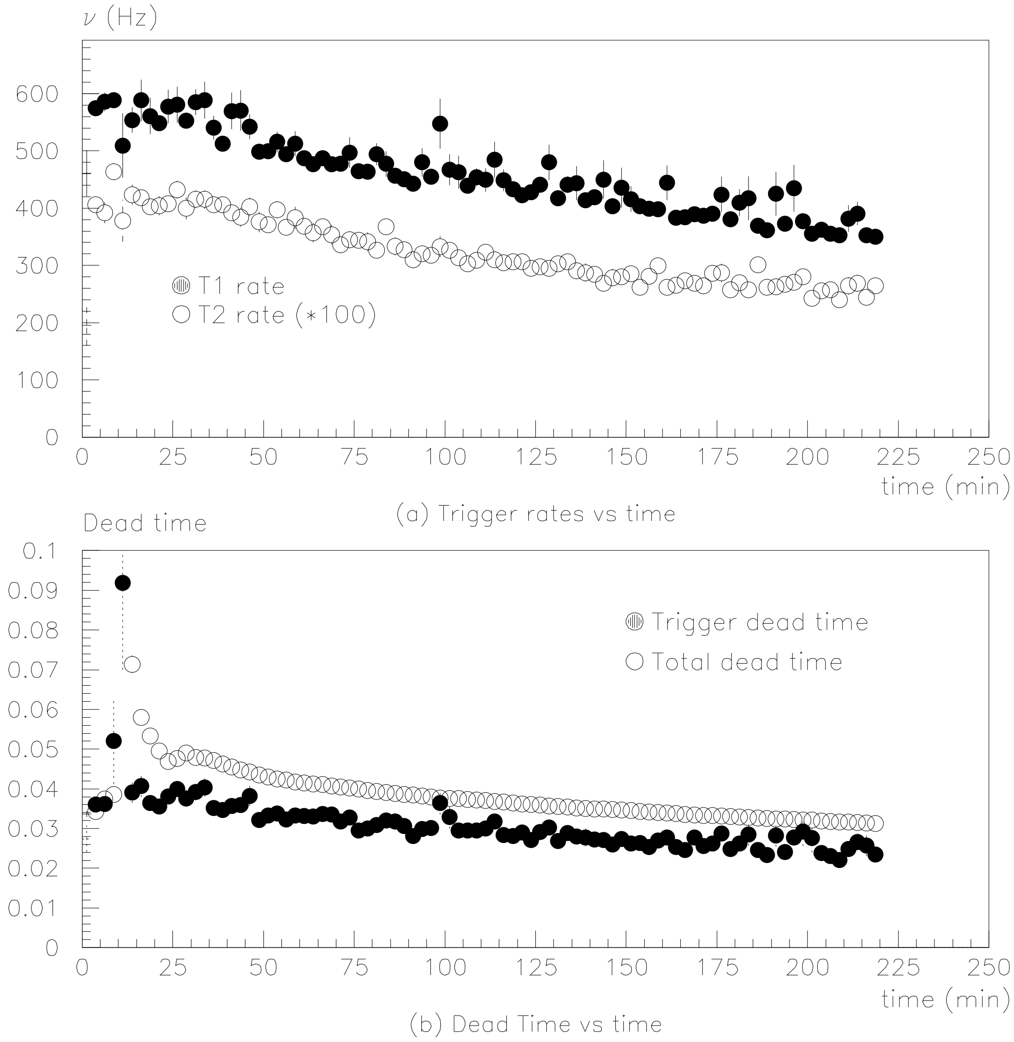

Figure 3: (a) First and second level trigger rates as function of the fill time for a typical fill of the 1998 data taking. The T2 rate has been multiplied by a factor 100. (b) Total and trigger induced dead times as function of the fill time.

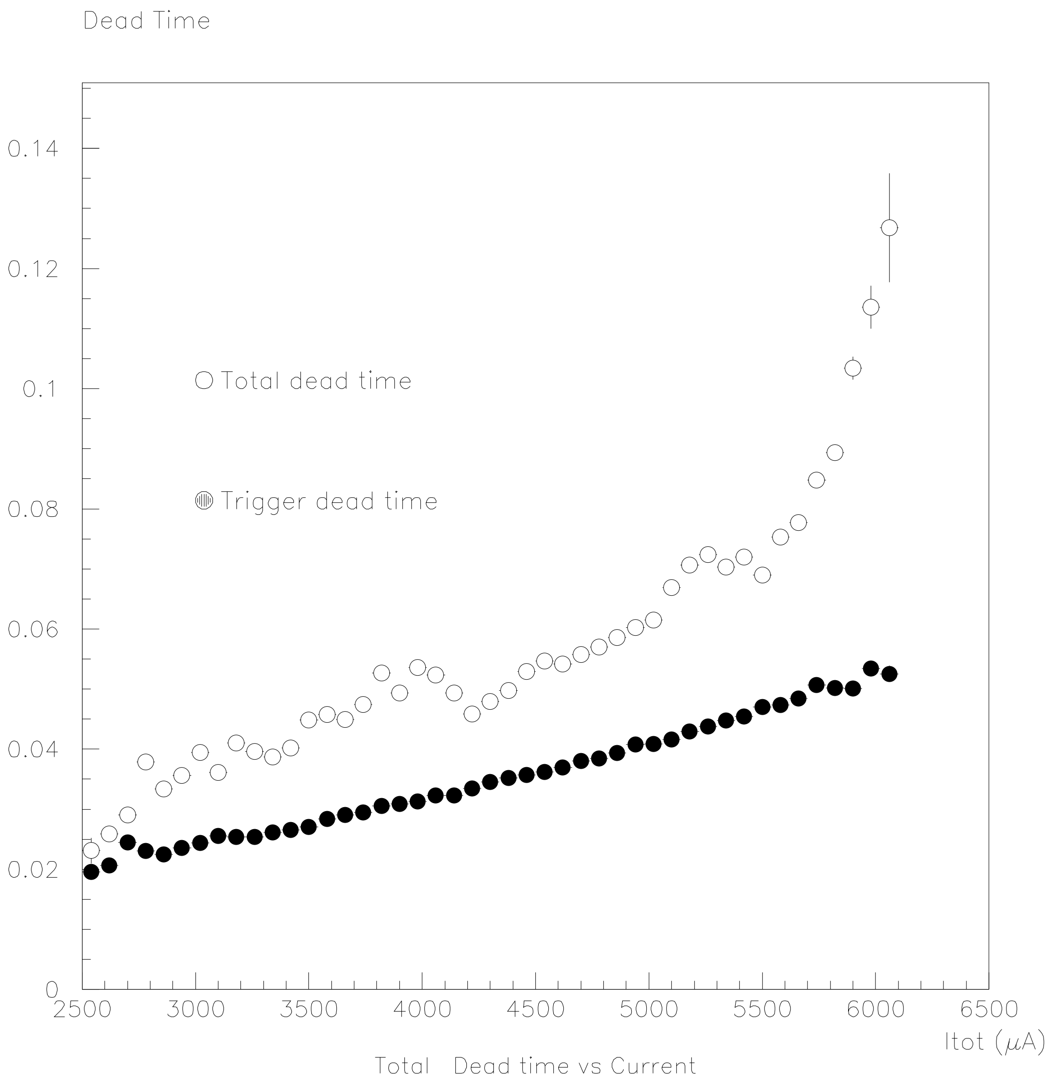

Figure 4: Total and trigger induced dead times as function of the total current in the machine for a typical 1998 run.

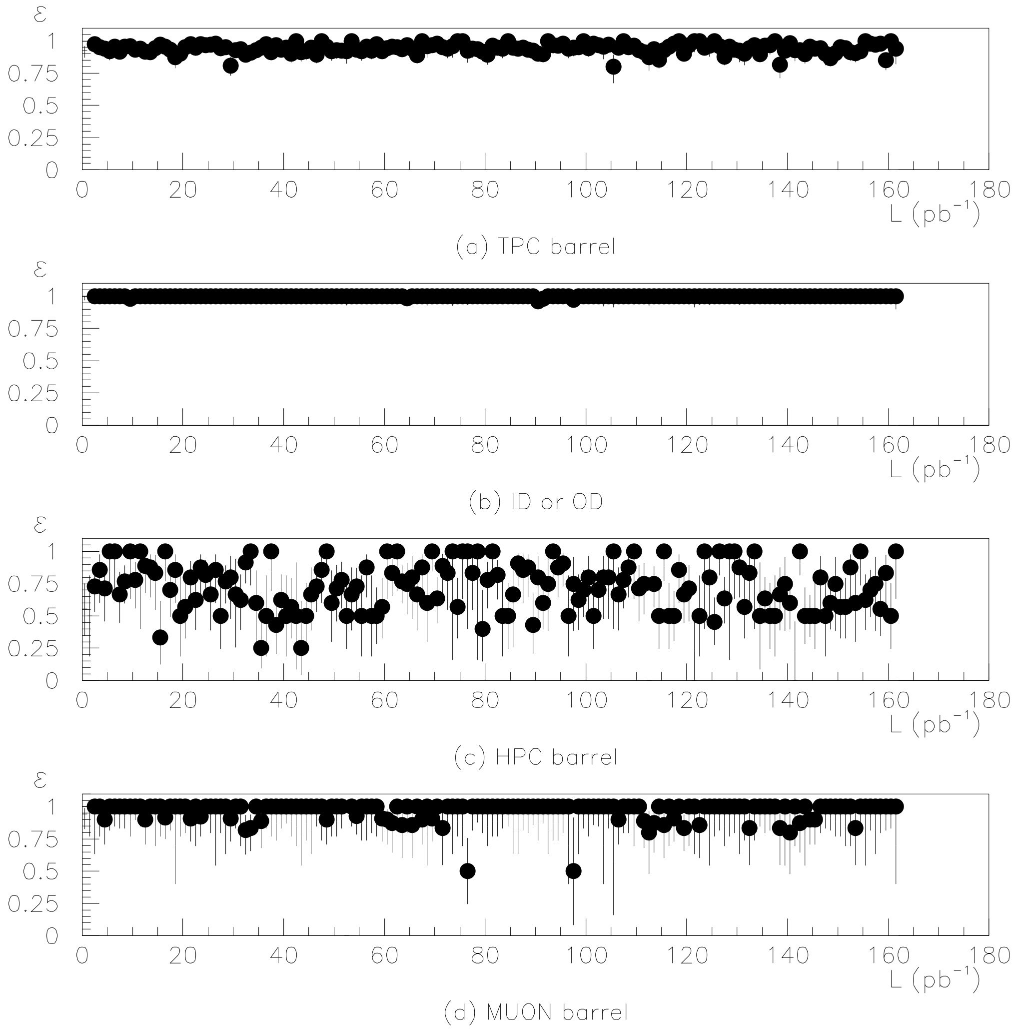

Figure 5: Subdetector trigger efficiency in the barrel region as function of the collected integrated luminosity. Each bin correspond $\sim 1\ pb^{-1}$. The plots correspond to 1998 data taking. The following kinematical cuts are also applied: (a,b) $P_t \geq 1GeV$, (c) $P \geq 5GeV$, (d) $P \geq 3GeV$.

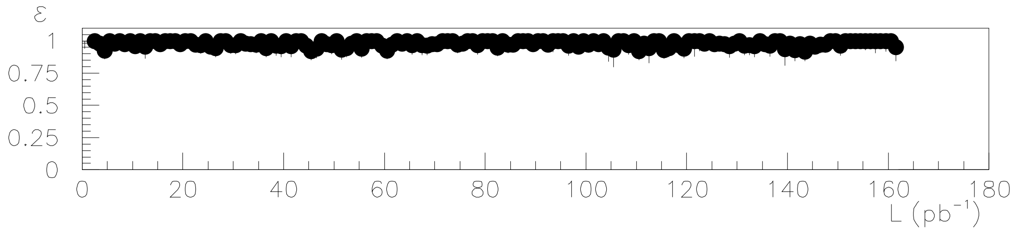

(a) TPC forward

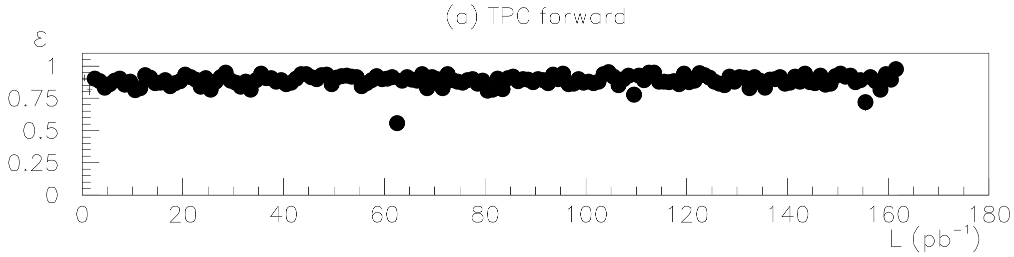

(b) FCH forward

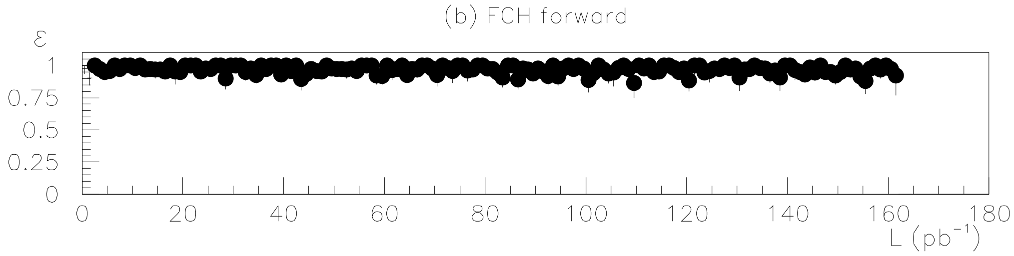

(c) MUON forward

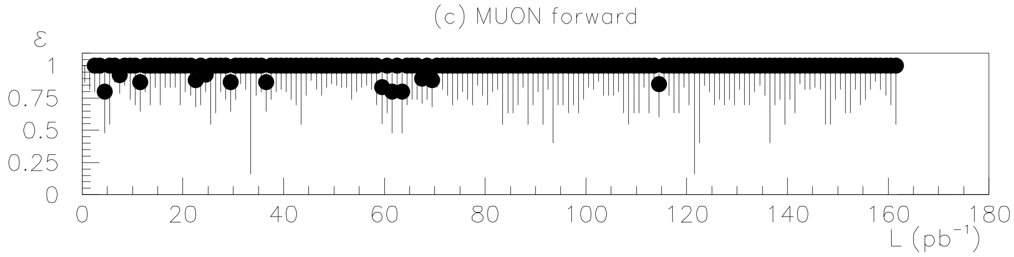

(d) FEMC forward

Figure 6: Subdetector trigger efficiency in the forward region as function of the collected integrated luminosity. Each bin correspond $\sim 1\ pb^{-1}$. The plots correspond to 1998 data taking. The following kinematical cuts are also applied: (a,b) $P_t \geq 3GeV$, (c) $P \geq 3GeV$, (d) $P \geq 5GeV$.

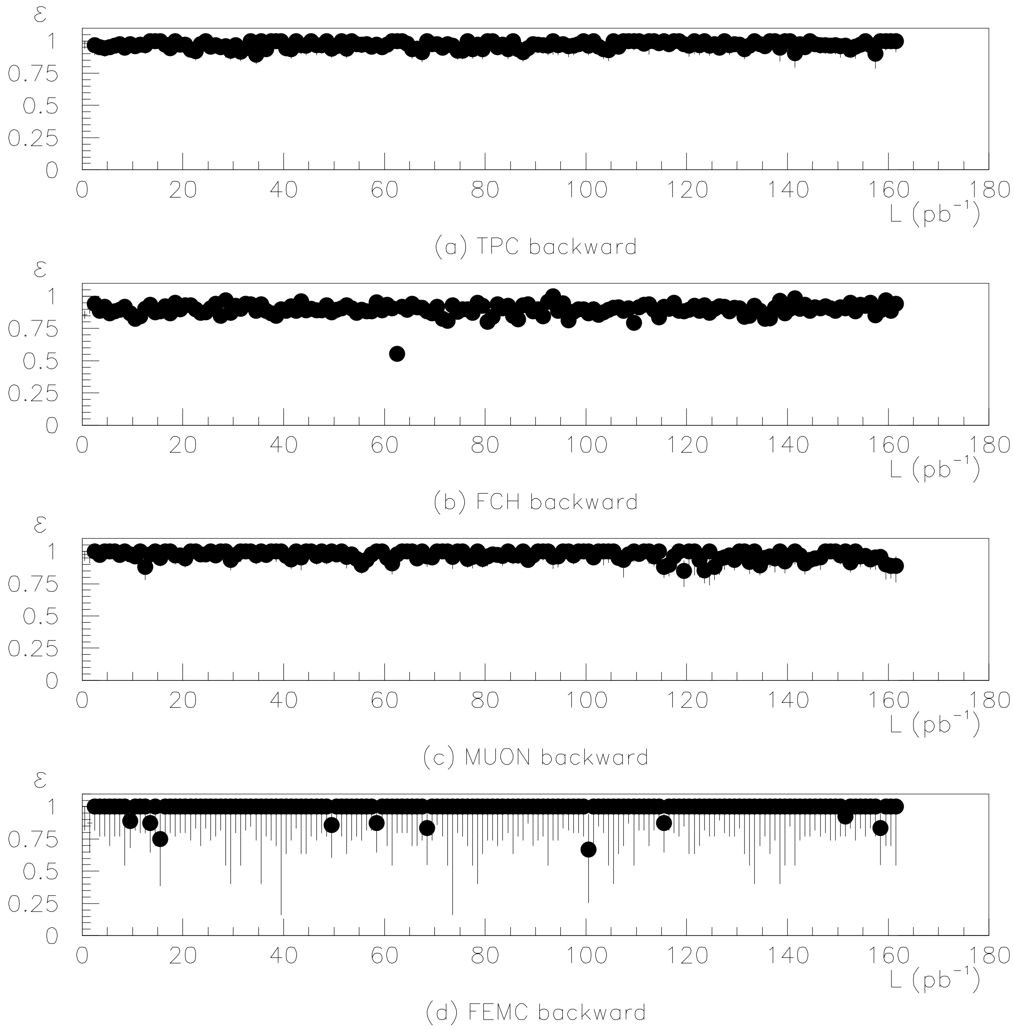

Figure 7: Subdetector trigger efficiency in the backward region as function of the collected integrated luminosity. Each bin correspond $\sim 1\ pb^{-1}$. The plots correspond to 1998 data taking. The following kinematical cuts are also applied: (a,b) $P_t \geq 3GeV$, (c) $P \geq 3GeV$, (d) $P \geq 5GeV$.

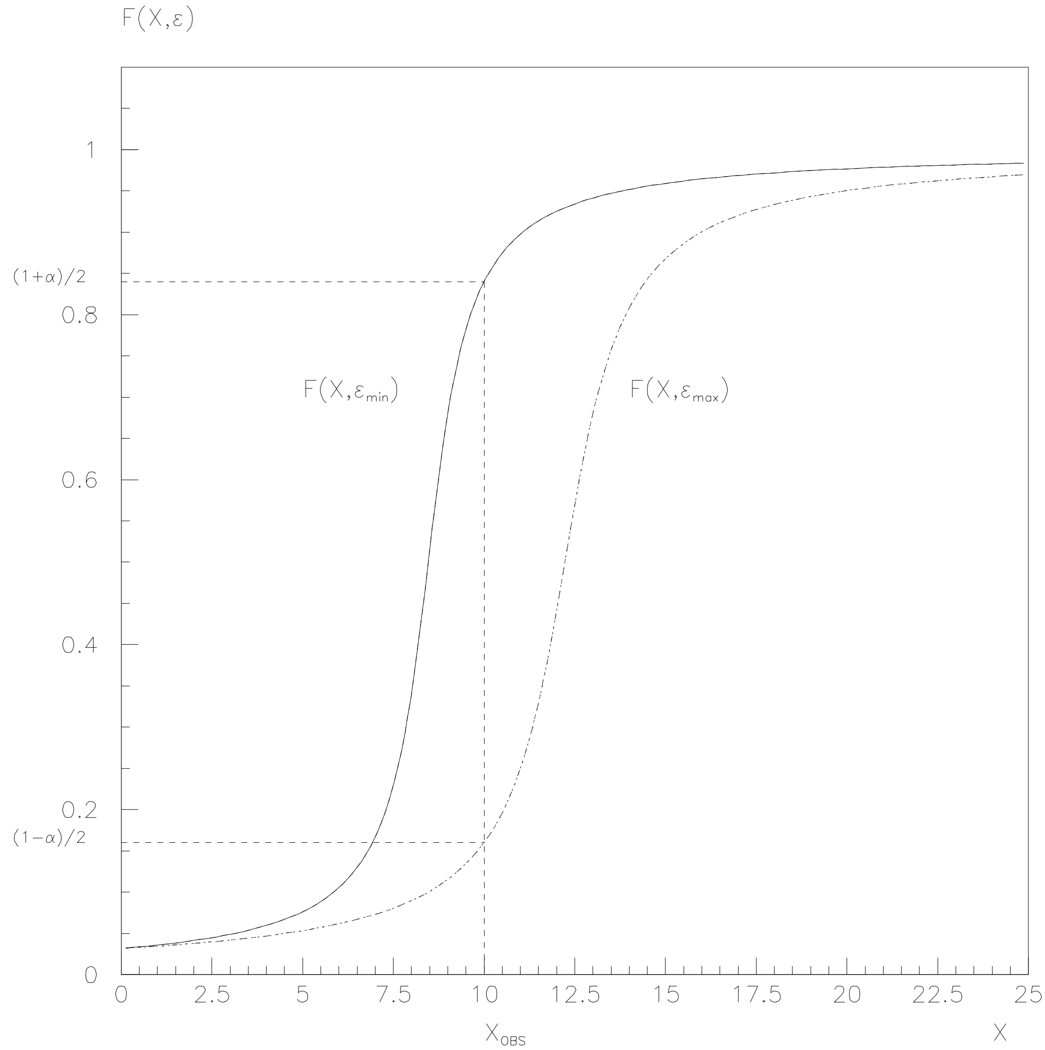

Figure 8: Graphical solution for the confidence interval determination. The construction of the central interval with probability α is shown. The measured value is x_m, and $F(x;\epsilon_{max})$, $F(x;\epsilon_{min})$ are the cumulative distributions with the unknow parameters $[\epsilon_{min}, \epsilon_{max}]$ to be estimated.

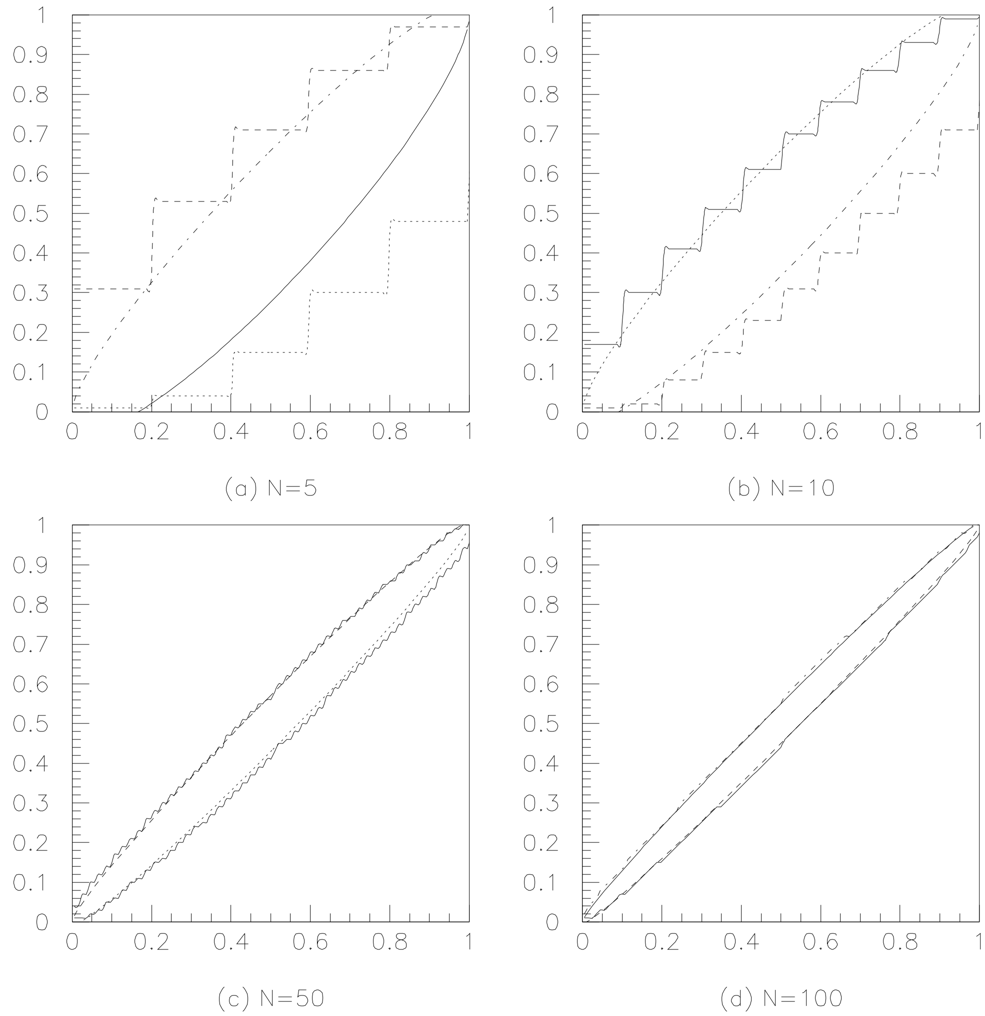

Figure 9: The 68% confidence belt for the binomial distribution with total number of events equal to: (a) $N_T = 5$, (b) $N_T = 10$, (c) $N_T = 50$ and (d)$N_T = 100$. The step behaviour is related to the discrete characteristic of the binomial p.d.f.. The interval approximating the errors with the variance is also shown superimposed.

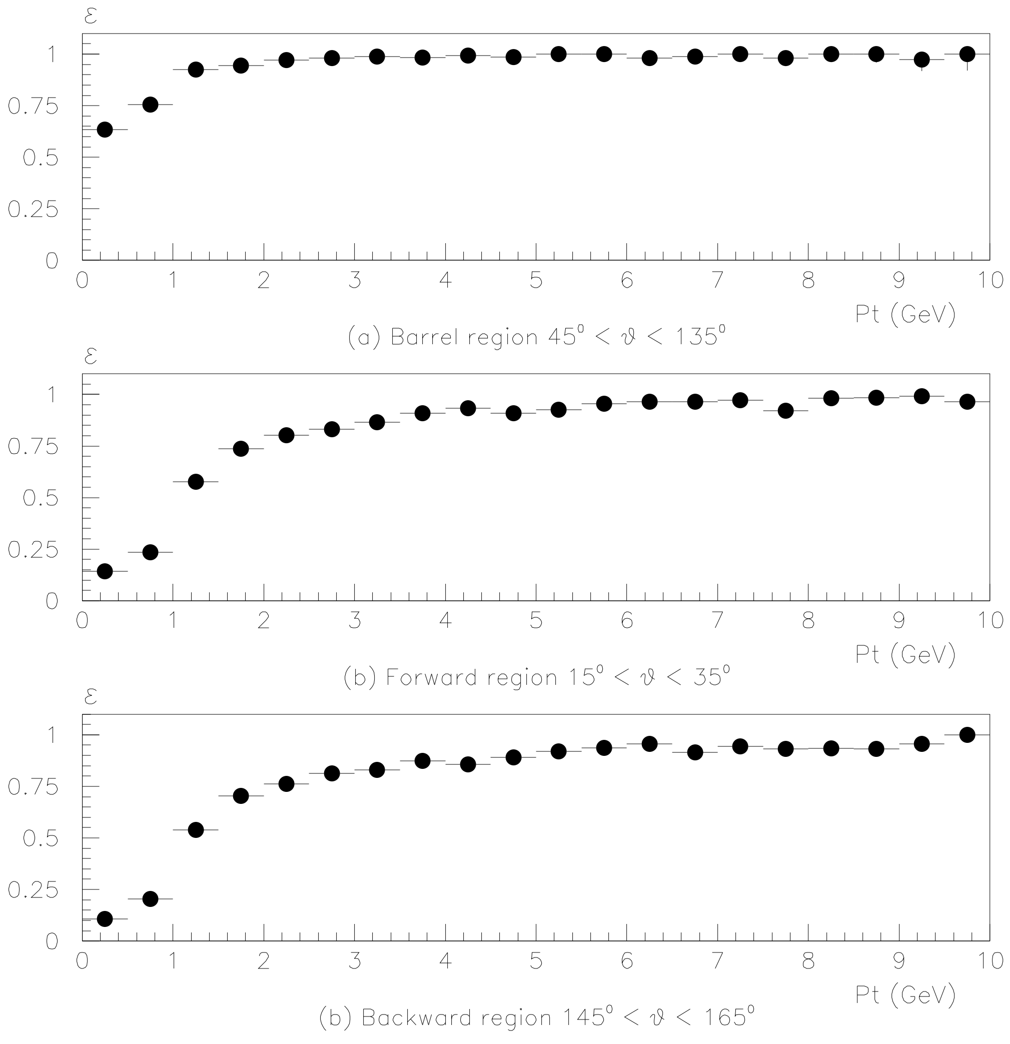

Figure 10: Single track efficiency vs momentum.

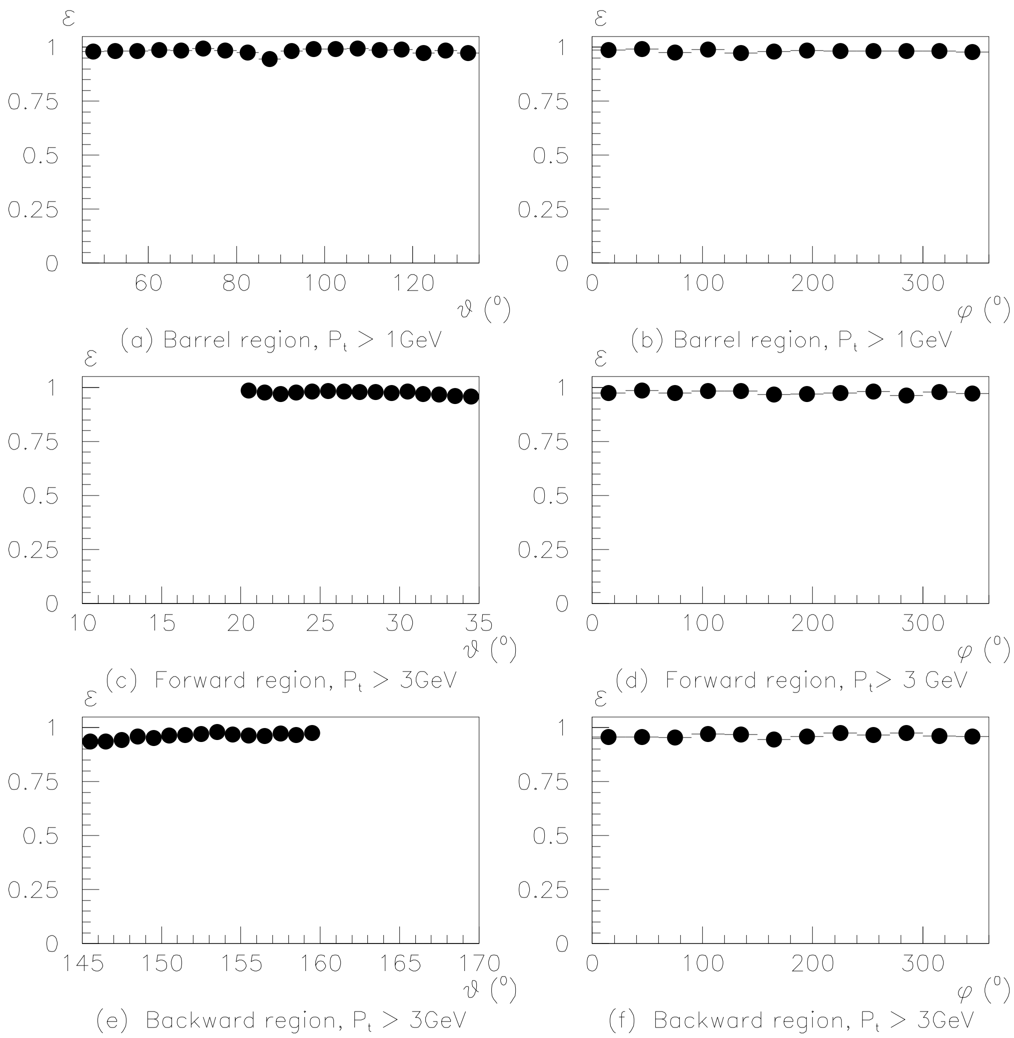

Figure 11: Single track efficiency vs polar angles.

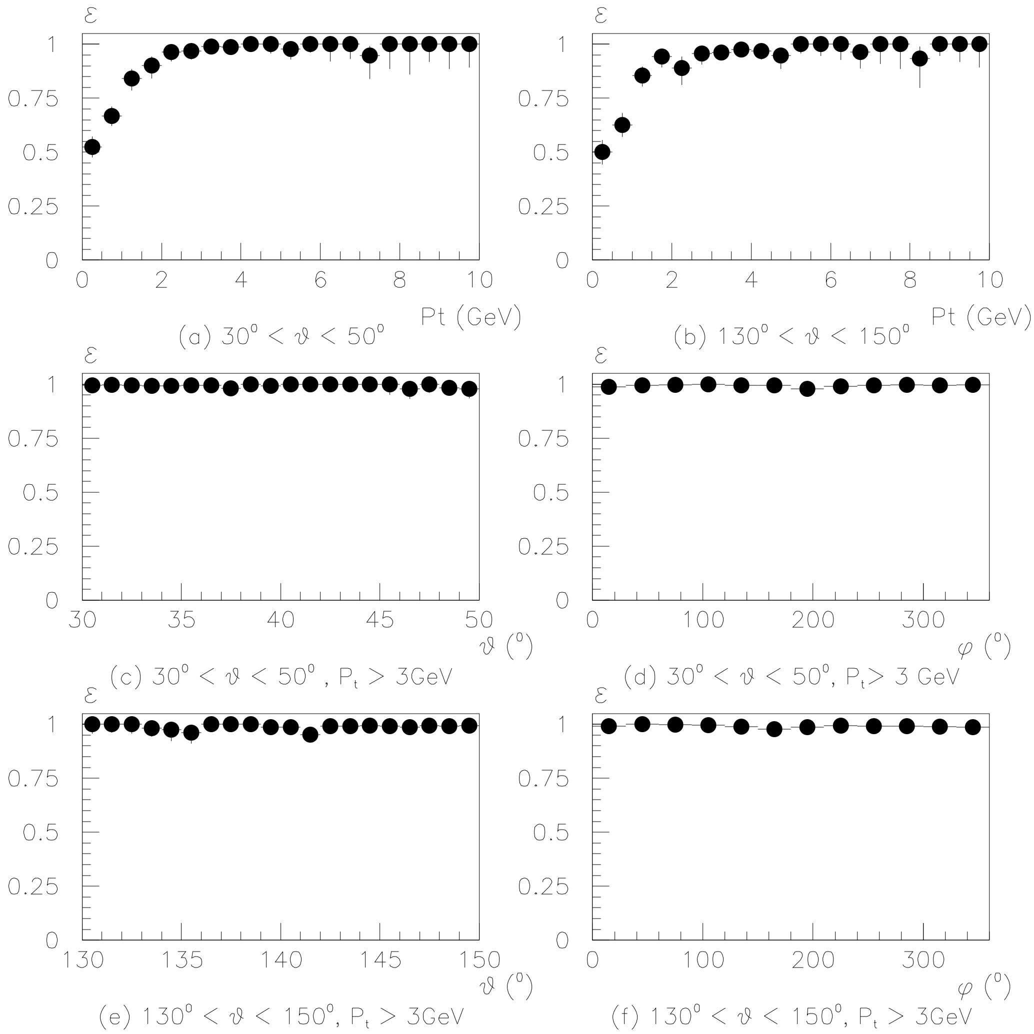

Figure 12: Single track efficiency for intermediate azimuthal angles.

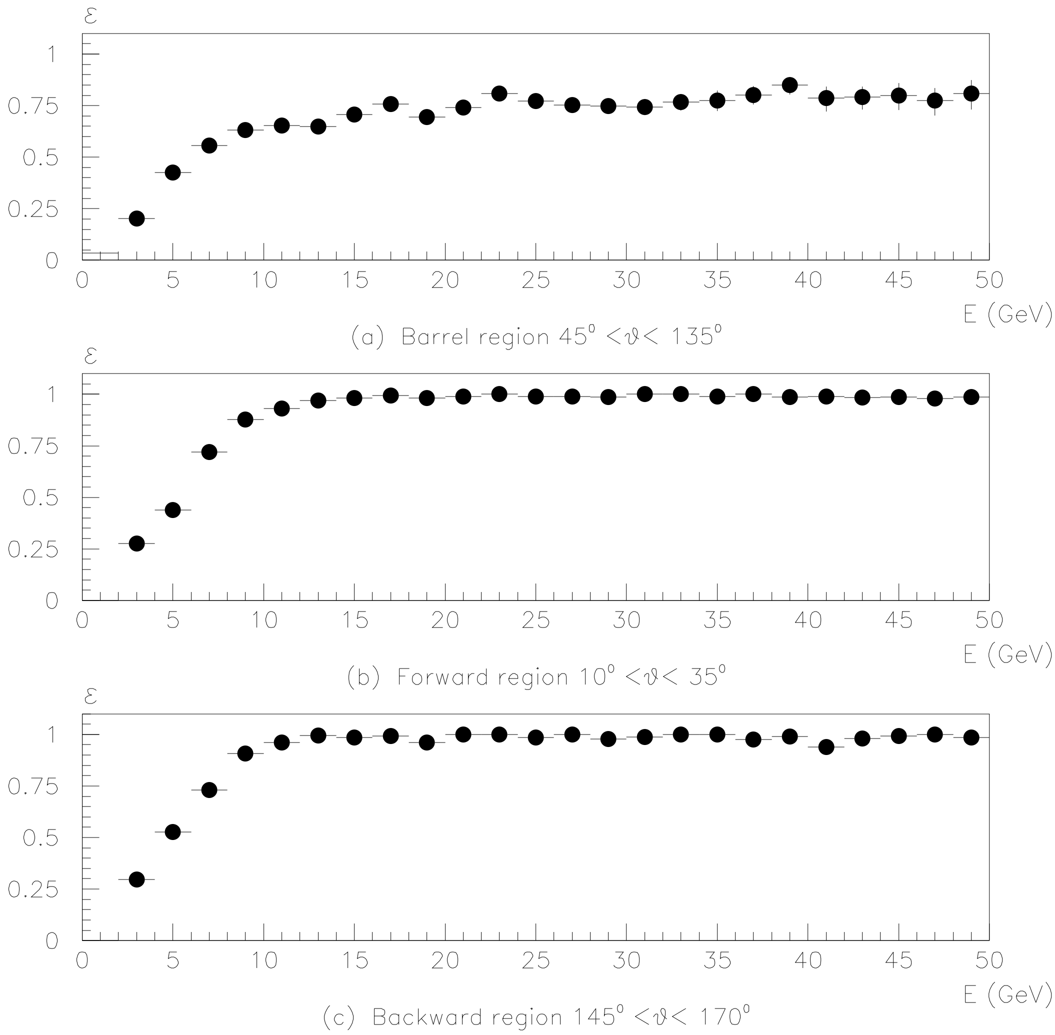

Figure 13: Single photon efficiencies.

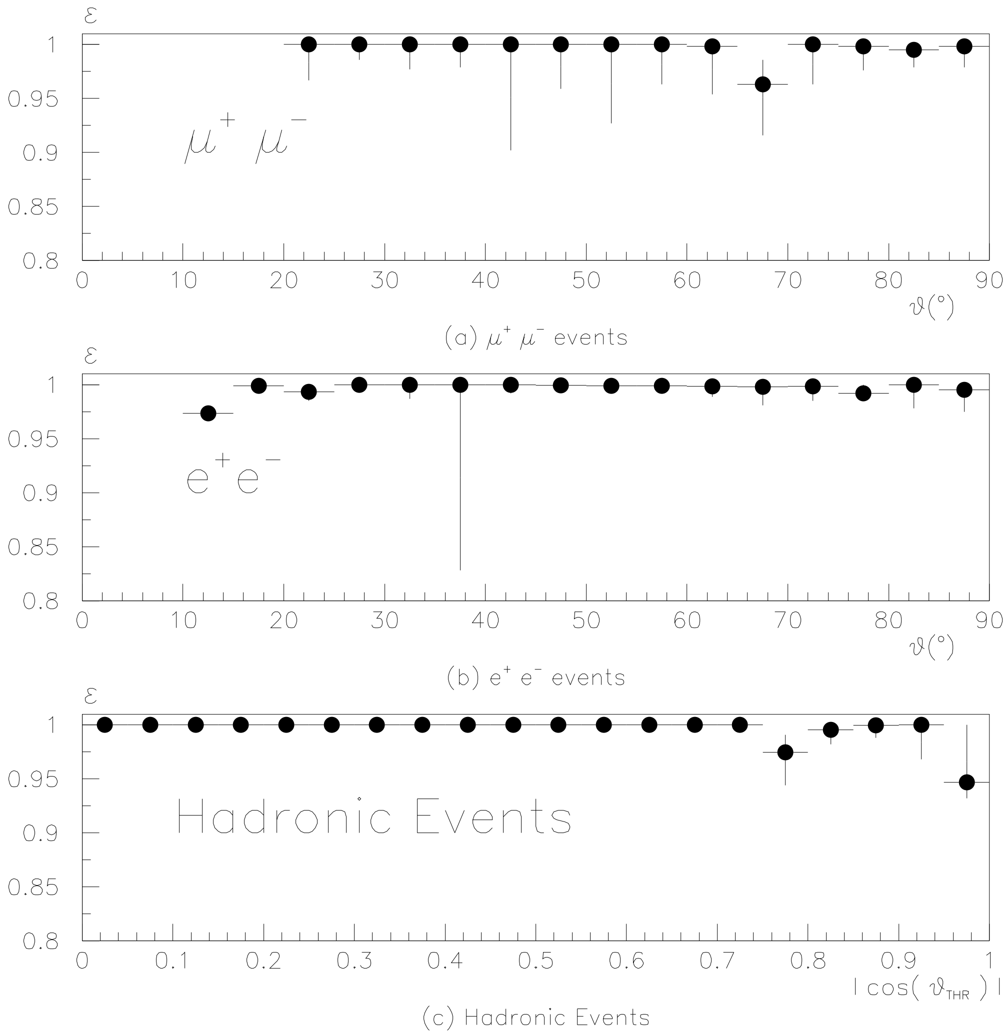

Figure 14: Trigger efficiency as a function of the polar angle for: (a) e^+e^-, (b) $\mu^+\mu^-$, (c) Hadronic events. Results correspond to 1998 data.

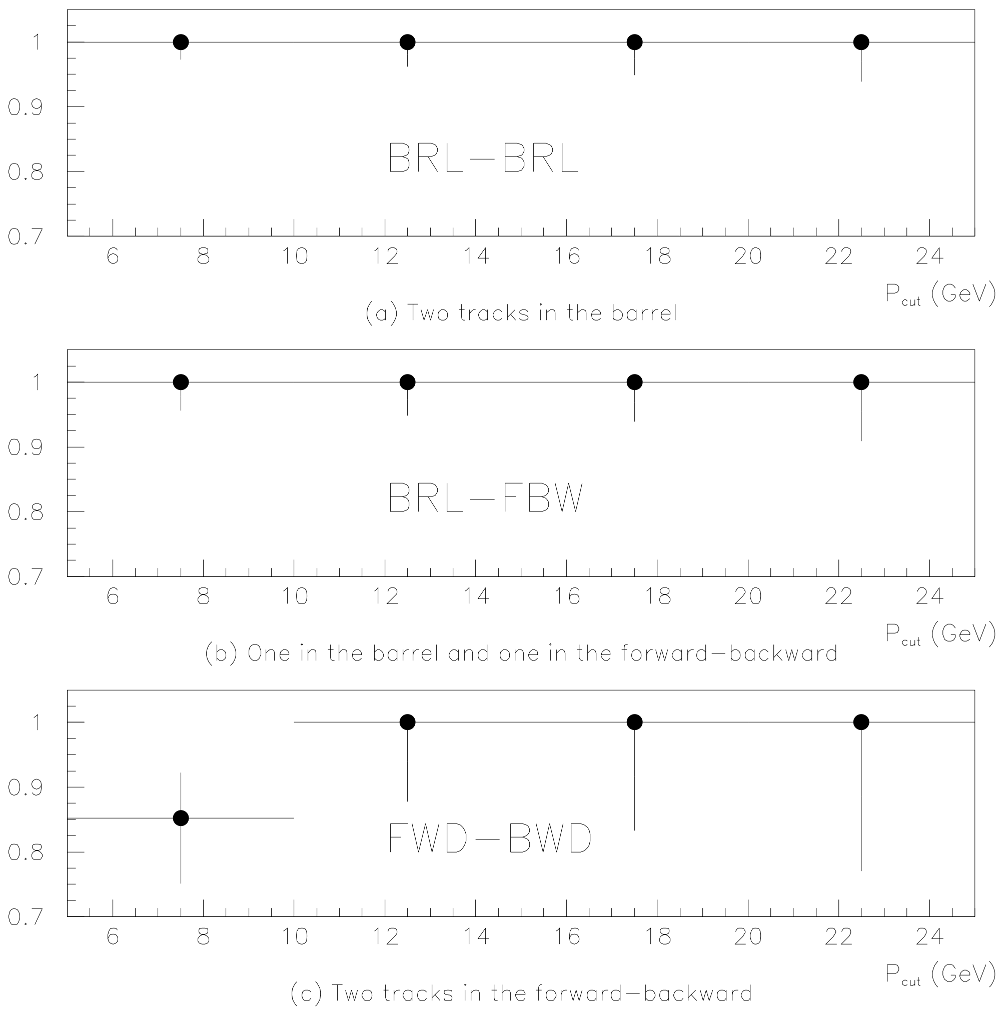

Figure 15: Trigger efficiency for events with two high energy tracks as function of the momentum cut: (a) BRL-BRL topology, (b) BRL-FWB topology, (c) FWD-BWD topology. Results correspond to 1997 data.

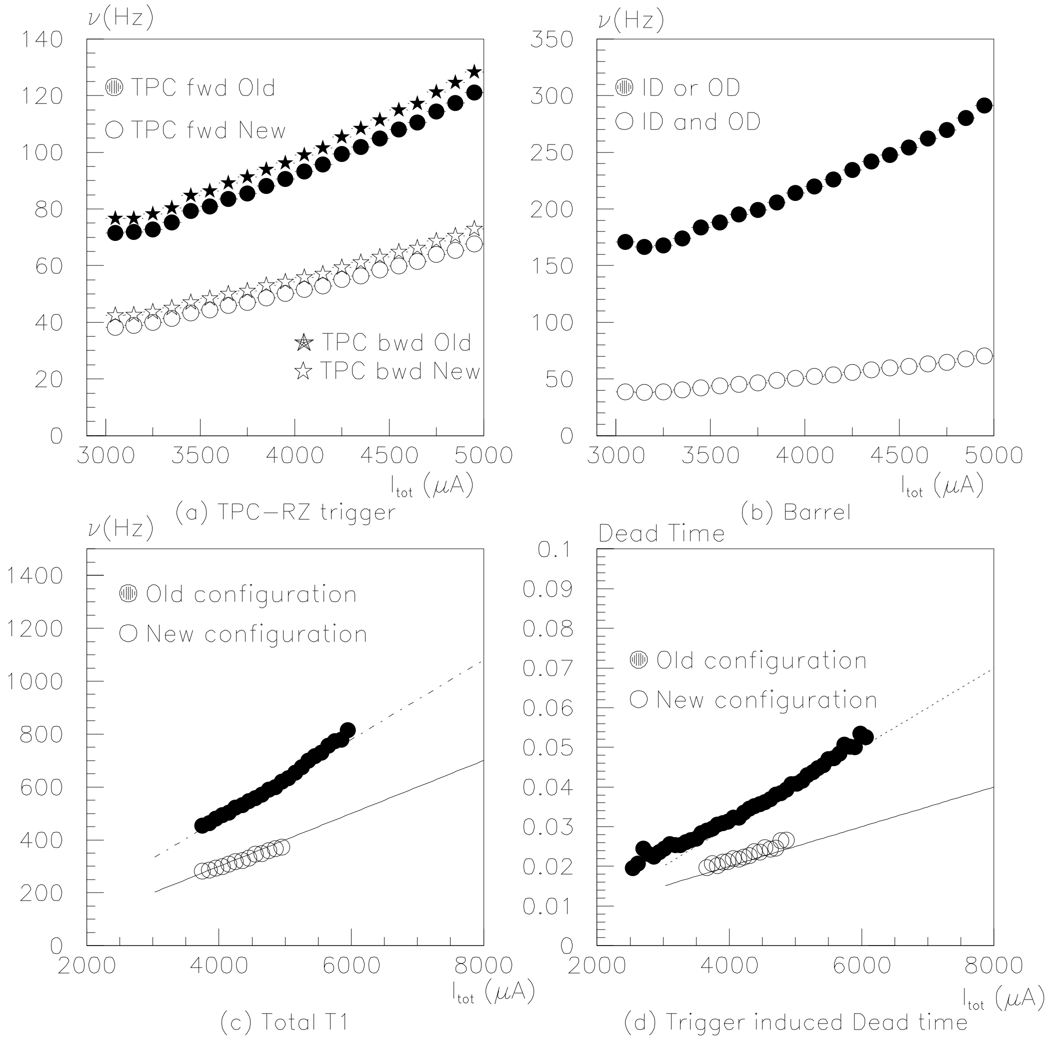

Figure 16: Trigger rates as function of the total current for "new" first level configurations: (a) TPC-RZ trigger, (b) Barrel region, (c) Total first level, (d) Trigger induced dead time.

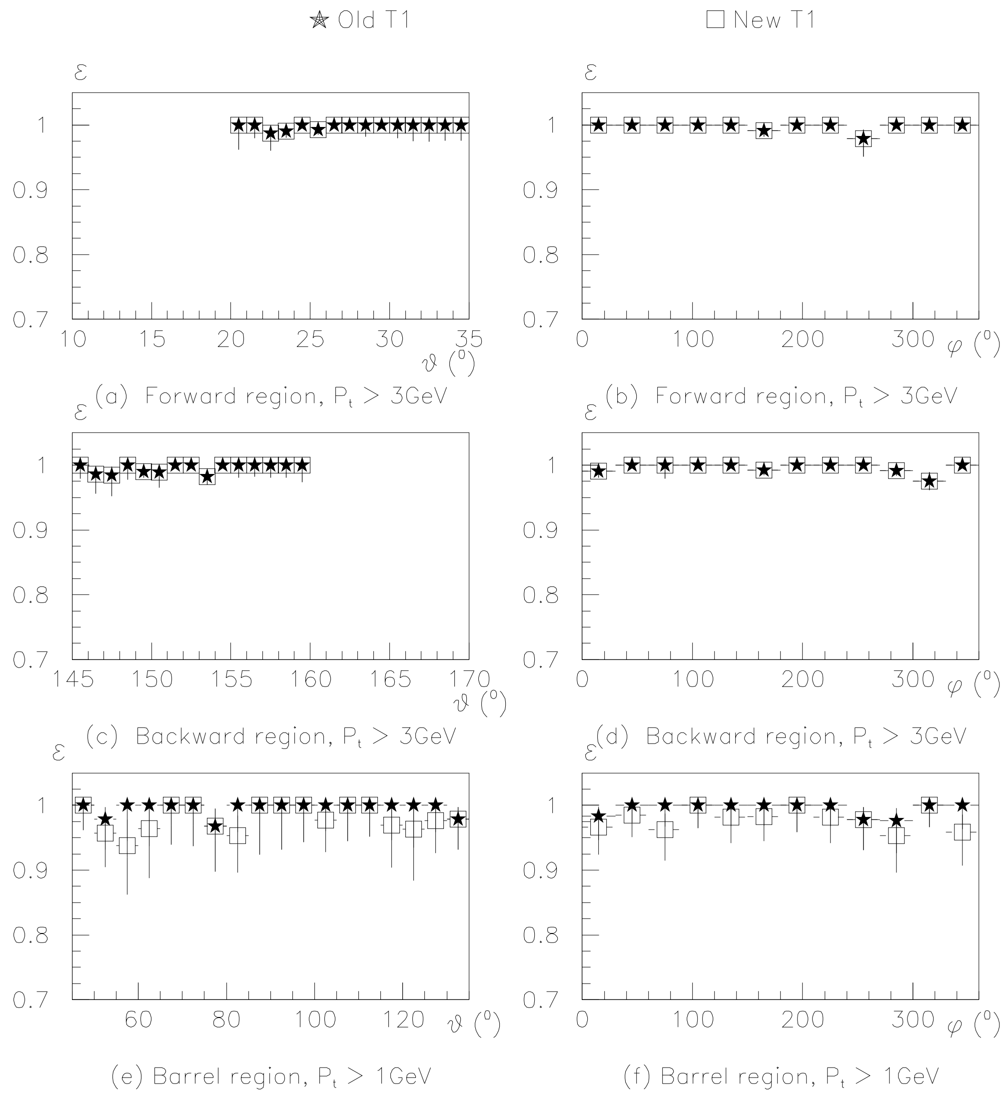

Figure 17: Comparison of the single track efficiencies of the "new" and "old" T1 configuration for the angular regions: (a,b) forward, (c,d) backward, (d,e) barrel. A transverse momentum cut is applied to the selected tracks.

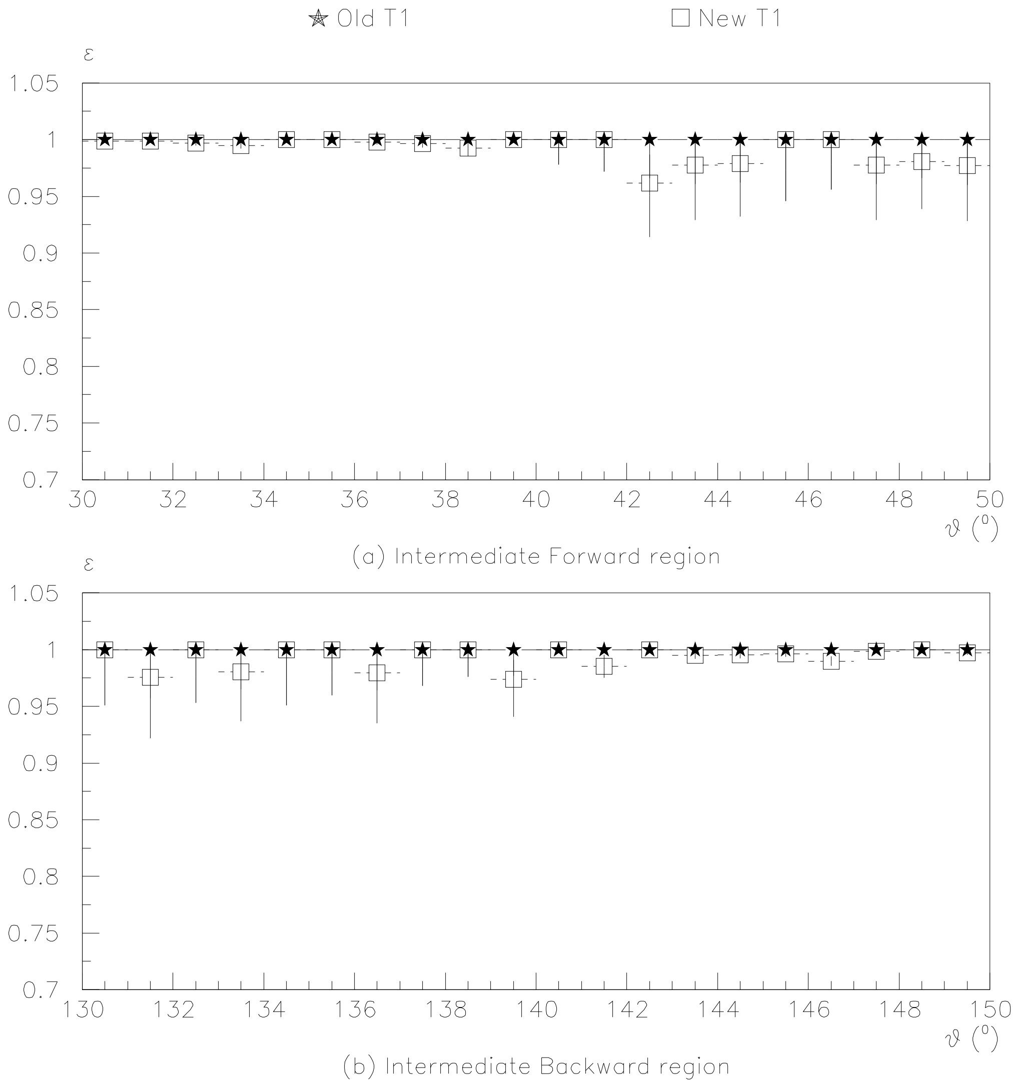

Figure 18: Comparison of the single track efficiencies of the "new" and "old" T1 configuration for the angular regions: (a,b) forward, (c,d) backward, (d,e) barrel. $P_t \geq 1GeV$ is required for the selected tracks.